


# Algorithms for variational Monte Carlo calculations of fermion projected entangled pair states in the swap gates formulation and the detailed balance of tensor network sequential sampling

Yantao Wu(武琰涛) and Zhehao Dai(戴哲昊)
**Citation:**Chin. Phys. B, 2026, 35 (**2**): 020502. DOI: 10.1088/1674-1056/ae2673
http://cpb.iphy.ac.cn; http://iopscience.iop.org/cpb

**What follows is a list of articles you may be interested in**

---

## High Chern number phase in topological insulator multilayer structures: A Dirac cone model study

Yi-Xiang Wang(王义翔) and Fu-Xiang Li(李福祥)
Chin. Phys. B, 2022, 31 (**9**): 090501. DOI: 10.1088/1674-1056/ac6b2e

## Thermodynamic properties of two-dimensional charged spin-1/2 Fermi gases

Jia-Ying Yang(杨家营), Xu Liu(刘旭), Ji-Hong Qin(秦吉红), and Huai-Ming Guo(郭怀明)
Chin. Phys. B, 2022, 31 (**6**): 060504. DOI: 10.1088/1674-1056/ac4e0b

## Impurity-induced Shiba bound state in the BCS-BEC crossover regime of two-dimensional Fermi superfluid

Siqi Shao(邵思齐), Kezhao Zhou(周可召), Zhidong Zhang(张志东)
Chin. Phys. B, 2019, 28 (**7**): 070501. DOI: 10.1088/1674-1056/28/7/070501

## Three-dimensional spin–orbit coupled Fermi gases: Fulde–Ferrell pairing, Majorana fermions, Weyl fermions, and gapless topological superfluidity

Xia-Ji Liu, Hui Hu, Han Pu
Chin. Phys. B, 2015, 24 (**5**): 050502. DOI: 10.1088/1674-1056/24/5/050502

---

**RAPID COMMUNICATION**

# Algorithms for variational Monte Carlo calculations of fermion projected entangled pair states in the swap gates formulation and the detailed balance of tensor network sequential sampling

Yantao Wu(武琰涛)[1,†] and Zhehao Dai(戴哲昊)[2]

[1] *Institute of Physics, Chinese Academy of Sciences, Beijing* 100190, *China*
[2] *Department of Physics and Astronomy, University of Pittsburgh, PA* 15213, *USA*

(Received 20 September 2025; revised manuscript received 27 November 2025; accepted manuscript online 2 December 2025)

In recent years, variational Monte Carlo (VMC) calculations of projected entangled pair states (PEPS) have emerged as a competitive method for computing the ground states of many-body quantum systems. This approach is particularly important for fermionic systems, where sign problems are prevalent. We derive and explain the algorithms for VMC calculations of fermionic PEPS within the swap-gates formulation. As a separate key result, we prove the detailed balance for sequential sampling of tensor networks.

**Keywords:** fermion systems and electron gas, computational techniques

**PACS:** 05.30.Fk, 02.70.-c

**DOI:** 10.1088/1674-1056/ae2673 **CSTR:** 32038.14.CPB.ae2673

## 1. Introduction

Numerical computation of ground states of two-dimensional many-body fermion systems is a fundamental problem in condensed matter physics. Due to fermion exchange, sign problems are prevalent in quantum Monte Carlo simulations[1] for fermions, making the method challenging for a broad range of signful systems. Based on the variational principle of energy, variational calculations using a wavefunction ansatz can potentially provide a better alternative for signful systems, if challenges in representation and optimization are overcome. In one dimension, a fermion system can be mapped to a system of hard-core bosons via the Jordan–Wigner (JW) transformation,[2] which can then be variationally solved using matrix product states (MPS) as the wavefunction ansatz, optimized via the density matrix renormalization group algorithm.[3]

In two dimensions, the JW transformation introduces non-locality; an alternative wavefunction ansatz that preserves locality in fermion systems is more suitable for representing ground states of local Hamiltonians. Fermion projected entangled pair states (fPEPS)[4–7] are designed for this purpose: given an fPEPS state, if a local operator supported in region $R$ acts on the state, only the tensors within $R$ are affected. The initial formulation of fPEPS is based on virtual fermions living on the virtual bonds of the PEPS. Later, equivalent formulations based on swap gates[8,9] or Grassmann numbers[10,11] have also been adopted to study fPEPS.

Optimizing a PEPS for the ground states of strongly correlated systems[12,13] remains a long-standing challenge in the field. Recently, variational Monte Carlo (VMC) optimization has emerged as the method yielding the lowest computed ground state energies for several challenging systems.[14–19] In particular, it has achieved the state-of-the-art result for the fermion Hubbard model at $\frac{1}{8}$ hole doping,[11] a particularly challenging and important regime. In the appendix of Ref. [11], the VMC algorithm is explained for fPEPS in the Grassmann formulation. However, the Grassmann formulation requires subtle reimplementations of tensor network operations, and it is not entirely clear how to adapt it to fPEPS implementations written in the swap gates formulation, one of the simplest formulations used in the field. Here, we derive and demonstrate the VMC algorithm in the swap gates formulation, and explicitly spell out the implementation of fermion sign in each step of the algorithm.

Crucially, as we explain the sampling algorithm, we also prove the detailed balance of sequential sampling of PEPS,[20] which has remained unclear and unproved until now.

This paper is organized as follows. In Section 2, we explain fPEPS in the swap gates formulation. In Section 3, we explain the VMC algorithm of fPEPS and prove the detailed balance of sequential sampling. In Section 4, we demonstrate the VMC results for certain representative fermion systems. In Section 5, we provide discussion and conclusions.

[†]Corresponding author. E-mail: yantaow@iphy.ac.cn

© 2026 Chinese Physical Society and IOP Publishing Ltd. All rights, including for text and data mining, AI training, and similar technologies, are reserved.

## 2. fPEPS in the swap gates formulation

### 2.1. Spinless fermions

The tensor product structure of the many-body fermion Hilbert space can be established by mapping it to a (hard-core) boson Hilbert space via prescribing an order to the fermion modes, equivalent to using a JW string. On a square lattice, in the swap gates formulation, the ordering of the fermion modes is shown in Fig. 1. One first extends the physical legs of all tensors towards the bottom-left and terminates them outside the network, then orders the fermion modes starting from the top-left tensor, counter-clockwise, until reaching the bottom-right tensor. This defines the computational basis of the many-fermion Hilbert space

$$|\boldsymbol{s}\rangle \equiv c_1^{\dagger s_1} c_2^{\dagger s_2} \cdots c_{N-1}^{\dagger s_{N-1}} c_N^{\dagger s_N} |\mathrm{vac}\rangle, \tag{1}$$

where $s_i = 0$ or 1 specifies whether the $i$-th fermion mode is occupied or not. $N$ is the total number of complex fermion modes, and $|\mathrm{vac}\rangle$ is their common vacuum.

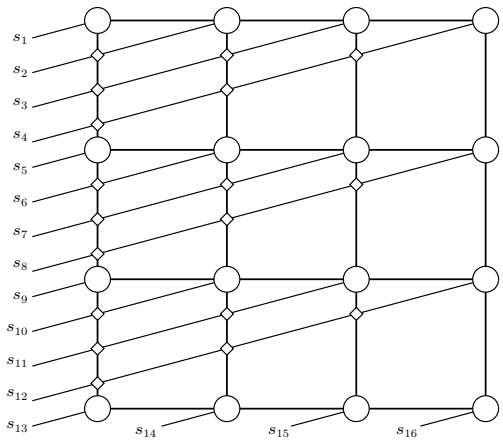
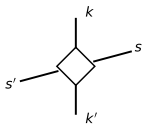



**Fig. 1.** A $4\times4$ fermion PEPS with swap gates.

An fPEPS is composed of $\mathbb{Z}_2$-symmetric tensors, where each virtual leg, indexed by $k = 1,2,\ldots,D$, carries a parity charge $P_k = 0$ or 1. At every site $i$, the five-leg fPEPS tensor is required to have even parity

$$A[i]^s_{lrdu} = 0 \text{ if } P_l + P_r + P_d + P_u \neq P_s \bmod 2, \tag{2}$$

where $l,r,d,u$ denote the indices for the left, right, down, and up virtual legs of $A$ at site $i$. The physical leg $s$ is extended towards the bottom-left, and each time it crosses another leg with index $k$, a swap gate is inserted




$$= (-1)^{P_s P_k} \delta_{kk'} \delta_{ss'}. \tag{3}$$

An fPEPS state $|\Psi\rangle$ is defined via its amplitude in the basis $|\boldsymbol{s}\rangle$: $\langle \boldsymbol{s}|\Psi\rangle$ equals the contraction of the 2D swap-gates-decorated tensor network, with physical indices projected to $\boldsymbol{s}$.

The fPEPS defined above has two key features.

(i) Well-definedness: as a physical leg is extended, there are multiple ways by which virtual bonds are crossed. These different ways are equivalent due to the gauge constraint Eq. (2).

(ii) Locality: when acted upon by a fermion operator in a local region, even if separated by a long JW string, e.g., $c_5^\dagger c_9$ in Fig. 1, only the tensors within that local region are affected.

See the appendix of Ref. [21] for a detailed explanation. In our algorithm, we adopt the configuration drawn in Fig. 1, where physical legs are bent flat enough so that they only cross vertical virtual legs and do not cross each other.

Computing the amplitude $\langle \boldsymbol{s}|\Psi\rangle$ is the core of the VMC algorithm, as explained in the next section.

### 2.2. Spinful fermions

For spinful fermions, the local physical dimension is 4: $s_i = (s_{i\uparrow}, s_{i\downarrow})$, and the fermion modes in $|\boldsymbol{s}\rangle$ are ordered as $s_{1\uparrow}, s_{1\downarrow}, s_{2\uparrow}, s_{2\downarrow}, \ldots$. One can encode $|00\rangle, |\uparrow 0\rangle, |\uparrow\downarrow\rangle, |0\downarrow\rangle$ as $s = 0,1,2,3$, so that the parity $P_s = s \bmod 2$.

### 2.3. Number conservation

In the sampling framework, a definite particle number $M$ can be imposed by sampling only over product states $\boldsymbol{s}$ with particle number equal to $M$. This approach is equivalent to computing the properties of $P_M|\Psi\rangle$ instead of $|\Psi\rangle$, where $P_M$ is the projector onto the total number sector $M$. Implementing the projector via sampling instead of tensors increases the representability of the variational ansatz over the bare fPEPS. We adopt number conservation in this way in Section 4.

## 3. VMC of fPEPS

In VMC, the expectation value of an operator $K$ is calculated as

$$\frac{\langle\Psi|K|\Psi\rangle}{\langle\Psi|\Psi\rangle} = \sum_{\boldsymbol{s}} \frac{|\langle \boldsymbol{s}|\Psi\rangle|^2}{\langle\Psi|\Psi\rangle} \frac{\langle \boldsymbol{s}|K|\Psi\rangle}{\langle \boldsymbol{s}|\Psi\rangle} \equiv \sum_{\boldsymbol{s}} p(\boldsymbol{s}) K_{\mathrm{loc}}(\boldsymbol{s}), \tag{4}$$

which is obtained by sampling $\boldsymbol{s}$ from the probability distribution $p(\boldsymbol{s}) = \frac{|\langle \boldsymbol{s}|\Psi\rangle|^2}{\langle\Psi|\Psi\rangle}$, and averaging over the estimator $K_{\mathrm{loc}}(\boldsymbol{s}) = \frac{\langle \boldsymbol{s}|K|\Psi\rangle}{\langle \boldsymbol{s}|\Psi\rangle}$.

To obtain $|\Psi\rangle$ as an approximate ground state of a Hamiltonian $H$, one performs optimization to minimize $\frac{\langle\Psi|H|\Psi\rangle}{\langle\Psi|\Psi\rangle}$ based on the gradients of $\langle H\rangle$ with respect to the complex conjugate[22] (denoted by an overhead bar) of the parameters $\theta_\alpha$ in the wavefunction ansatz

$$g_\alpha \equiv \frac{\partial \langle H\rangle}{\partial \overline{\theta_\alpha}} = [\overline{O_\alpha(\boldsymbol{s})} H_{\mathrm{loc}}(\boldsymbol{s})] - [\overline{O_\alpha(\boldsymbol{s})}][H_{\mathrm{loc}}(\boldsymbol{s})], \tag{5}$$

where $[\cdot]$ denotes statistical averaging with respect to $p(\boldsymbol{s})$. $O_\alpha(\boldsymbol{s})$ is the log-derivative of $\langle \boldsymbol{s}|\Psi\rangle$ with respect to $\theta_\alpha$

$$O_\alpha(\boldsymbol{s}) \equiv \frac{\partial \ln\langle \boldsymbol{s}|\Psi\rangle}{\partial\theta_\alpha} = \frac{\partial\langle \boldsymbol{s}|\Psi\rangle/\partial\theta_\alpha}{\langle \boldsymbol{s}|\Psi\rangle}. \tag{6}$$

Four subroutines are required in a VMC calculation:

(i) Computing the amplitude $\langle \boldsymbol{s}|\Psi\rangle$.

(ii) Computing the log-derivative $\frac{\partial\langle \boldsymbol{s}|\Psi\rangle/\partial\theta_\alpha}{\langle \boldsymbol{s}|\Psi\rangle}$.

(iii) Computing the local energy $\frac{\langle \boldsymbol{s}|H|\Psi\rangle}{\langle \boldsymbol{s}|\Psi\rangle}$.

(iv) A Monte Carlo update to sample $\boldsymbol{s}$ from $p(\boldsymbol{s})$.

We now detail the above in the context of fPEPS. We consider an fPEPS of size $L_x \times L_y$ and bond dimension $D$.

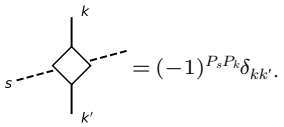
### 3.1. fPEPS tensors after sampling

For any given sample $\boldsymbol{s}$, the index of each physical leg at site $i$ is fixed to $s_i$. The 5-leg tensor $A[i]^s_{lrdu}$ then becomes a 4-leg tensor $\tilde{A}[i]_{lrdu} = A[i]^{s_i}_{lrdu}$, with total $\mathbb{Z}_2$ charge equal to $P_{s_i}$

$$\tilde{A}[i]_{lrdu} = 0, \text{ if } P_l + P_r + P_d + P_u \neq P_{s_i} \bmod 2. \tag{7}$$

Pictorially, the tensor after sampling is represented by changing the physical legs to dashed lines. A dashed line is no longer an index of the tensor, but a fixed number used to keep track of its $\mathbb{Z}_2$ charge. We draw it only when needed for swap gates.

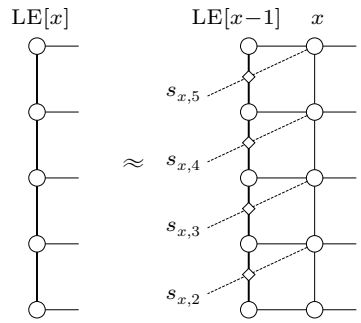
Correspondingly, for a given $s$, the swap gate reduces to a gate in the Hilbert space of the virtual leg




$$= (-1)^{P_s P_k}\delta_{kk'}. \tag{8}$$

### 3.2. Computation of the amplitude and the boundary MPS environment

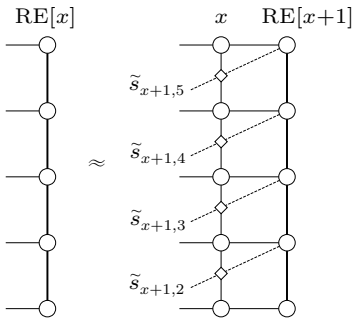
The amplitude $\langle \boldsymbol{s}|\Psi\rangle$ can be evaluated using boundary MPS (bMPS) contraction. This needs the bMPS left environments (`LE`) or right environments (`RE`). Both `LE` and `RE` are a list of bMPS with maximal bond dimension $D' > D$. `LE[0]` is taken as the trivial MPS, and `LE[x]` is then iteratively computed for $x = 1$ to $L_x$ as




(9)

where $s_{x,y}$ is the value of the sample at the coordinate $(x,y)$.

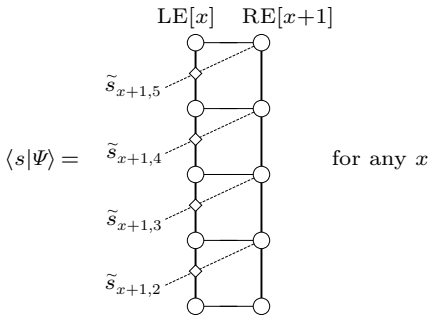
Similarly, `RE[Lx+1]` is the trivial MPS, and `RE[x]` is iteratively computed for $x = L_x$ to 1 as




(10)

where $\tilde{s}_{x,y} \equiv (\sum_{x'\geq x} s_{x,y}) \mod 2$ is the sample assoicated with `RE[x][y]`. It can be updated as $\tilde{s}_{x,y} = (s_{x,y} + \tilde{s}_{x+1,y}) \mod 2$.

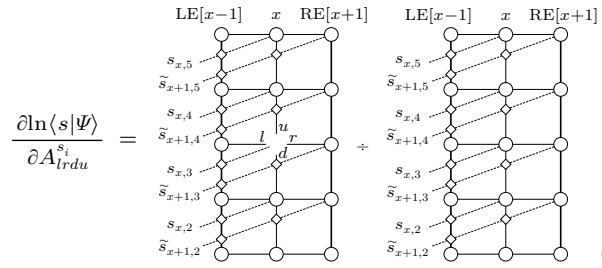
Equations (9) and (10) are both implemented via MPO-MPS variational compression with complexity $O(D'^3D^2 + D'^2D^4)$.[20] The amplitude is then computed as




(11)

### 3.3. Computation of the log-derivative

The variational parameters of an fPEPS are the $\mathbb{Z}_2$ symmetric tensors $A[i]^{p_i}_{lrdu}$ with $i$ labeling the sites. Given sample $\boldsymbol{s}$, the log-derivative of $\langle \boldsymbol{s}|\Psi\rangle$ with respect to $A[i]$ is 0 for $p_i \neq s_i$. For $p_i = s_i$, the log-derivative is computed as the contraction of the 2D network with a hole at site $i$




(12)

This can be contracted exactly with complexity $O(D'^3D^2 + D'^2D^4)$.

### 3.4. Computation of the local energy

Consider a short-range Hamiltonian with fermion hopping and an interaction diagonal in the basis $\boldsymbol{s}$. For diagonal terms $O$ in the Hamiltonian, the local energy is simply its diagonal element: $\frac{\langle \boldsymbol{s}|O|\Psi\rangle}{\langle \boldsymbol{s}|\Psi\rangle} = O_{\boldsymbol{s},\boldsymbol{s}}$. Thus, it suffices to compute the local energy for the hopping terms.

To compute $\frac{\langle \boldsymbol{s}|c_i^\dagger c_j|\Psi\rangle}{\langle \boldsymbol{s}|\Psi\rangle}$, one acts the hopping operator on $\langle \boldsymbol{s}|$ and properly accounts for the JW sign: $\langle \boldsymbol{s}|c_i^\dagger c_j =$

$(-1)^{\#_{ij}}\langle \boldsymbol{s}'|$, where $\#_{ij}$ is the number of fermions in $\boldsymbol{s}$ between (excluding) sites $i$ and $j$ along the JW string

$$\frac{\langle \boldsymbol{s}|c_i^\dagger c_j|\Psi\rangle}{\langle \boldsymbol{s}|\Psi\rangle} = (-1)^{\#_{ij}}\frac{\langle \boldsymbol{s}'|\Psi\rangle}{\langle \boldsymbol{s}|\Psi\rangle}. \tag{13}$$

Here, $\boldsymbol{s}'$ and $\boldsymbol{s}$ differ only locally, and $\langle \boldsymbol{s}|\Psi\rangle$ and $\langle \boldsymbol{s}'|\Psi\rangle$ should be computed using the same LE and RE.

### 3.5. Monte Carlo update

The locality of an fPEPS allows extensive reuse of LE and RE. For any neighboring sites $i$ and $j$, one can perform a 2-site local update: if a particle occupies exactly one of the two sites, swap the occupation and propose the post-swap configuration $\boldsymbol{s}'$, and accept $\boldsymbol{s}'$ with probability

$$\min\left\{1, \frac{|\langle \boldsymbol{s}'|\Psi\rangle|^2}{|\langle \boldsymbol{s}|\Psi\rangle|^2}\right\},$$

otherwise, do nothing and keep the current $\boldsymbol{s}$.

One MC sweep is defined as performing one 2-site local update for every nearest-neighbor vertical and horizontal bond on the lattice. The updates are performed sequentially: starting from the site $(x,y)=(1,1)$, then moving to $(1,2)$, and continuing up to $(1,L_y)$; next, moving to the column at $(2,1)$, and so on until reaching the top-right corner of the lattice. This procedure is called sequential sampling, first proposed in Ref. [20]. Its main advantage is the ability to reuse LE and RE during the MC sweep. The computational complexity of one MC sweep is $O(L_xL_yD'^2D^4)$.

It is, however, not immediately obvious that sequential sampling is reversible, i.e., satisfies detailed balance, due to the apparent ordering in the updates. This issue has remained unclear until now. In the next section, we prove that sequential sampling satisfies detailed balance, guaranteeing convergence to a unique stationary distribution $p(\boldsymbol{s})$, provided that the MC update is also irreducible and aperiodic.

### 3.6. Detailed balance of sequential sampling

Consider a system of $N$ spins or fermion modes. Let the sample space $\Omega$ be the product of $N$ local sample spaces $\Omega_i$. Let $\boldsymbol{s}=(s_1,s_2,\ldots,s_N)\in\Omega$, where $s_i\in\Omega_i$. Given the target probability distribution $\pi(\boldsymbol{s})$, the sequential sampling procedure is defined as follow:

**Algorithm 1**: Sequential sampling.

**for** $i\leftarrow 1$ **to** $N$ **do**
- Denote the spin configuration as $\boldsymbol{s}$
- Fix all spins excluding spin $i$: $\boldsymbol{s}_{\neq i}$
- Sample new spin $s_i'$ with transition probability $p_i(s_i\to s_i'|\boldsymbol{s}_{\neq i})$ that satisfies the conditional detailed balance, restricted to spin $i$:

$$p_i(s_i\to s_i'|\boldsymbol{s}_{\neq i})\pi(\boldsymbol{s}_{1:i-1},s_i,\boldsymbol{s}_{i+1:N}) = p_i(s_i'\to s_i|\boldsymbol{s}_{\neq i})\pi(\boldsymbol{s}_{1:i-1},s_i',\boldsymbol{s}_{i+1:N})$$

where $\boldsymbol{s}_{a:b}\equiv(s_a,s_{a+1},\ldots,s_b)$.

**Theorem 1** Algorithm 1 (sequential sampling) satisfies detailed balance with $\pi(\boldsymbol{s})$ as the stationary distribution.

**Proof** We take $N=3$ for notational simplicity. It is straightforward to see that the proof generalizes to arbitrary $N$. Consider $\boldsymbol{s}=(s_1,s_2,s_3)$ and $\boldsymbol{s}'=(s_1',s_2',s_3')$ before and after one step of sequential sampling. By conditional detailed balance:

$$\begin{aligned}
&p_1(s_1\to s_1'|s_2,s_3)\pi(\boldsymbol{s}) = p_1(s_1'\to s_1|s_2,s_3)\pi(s_1',\boldsymbol{s}_{2:3}),\\
&p_2(s_2\to s_2'|s_1',s_3)\pi(s_1',\boldsymbol{s}_{2:3}) = p_2(s_2'\to s_2|s_1',s_3)\pi(\boldsymbol{s}'_{1:2},s_3),\\
&p_3(s_3\to s_3'|s_1',s_2')\pi(\boldsymbol{s}'_{1:2},s_3) = p_3(s_3'\to s_3|s_1',s_2')\pi(\boldsymbol{s}').
\end{aligned}$$

Multiplying the three equations yields the detailed balance condition for sequential sampling:

$$p(\boldsymbol{s}\to\boldsymbol{s}')\pi(\boldsymbol{s}) = p(\boldsymbol{s}'\to\boldsymbol{s})\pi(\boldsymbol{s}'), \tag{14}$$

where $p(\boldsymbol{s}\to\boldsymbol{s}')$ denotes the transition probability from $\boldsymbol{s}$ to $\boldsymbol{s}'$ in one step of sequential sampling.

This proof naturally generalizes to the case where conditional sampling is performed over multiple sites in a local region instead of a single site.

### 3.7. Stochastic reconfiguration

To obtain the ground state in the context of VMC, one often employs the method of stochastic reconfiguration (SR), which we also adopt in Section 4. SR is extensively discussed in the literature [23], and its application to fPEPS is no different. We summarize the details here for completeness.

Let $\boldsymbol{\theta}$ be a complex vector containing all variational parameters in an fPEPS. Instead of performing steepest descent: $\theta_\alpha'=\theta_\alpha-\delta\cdot\frac{\partial\langle H\rangle}{\partial\overline{\theta_\alpha}}$, where $\delta$ is the step size (also called learning rate), one descends along a direction $\boldsymbol{X}$, i.e., $\boldsymbol{\theta}'=\boldsymbol{\theta}-\delta\cdot\boldsymbol{X}$, where $\boldsymbol{X}$ solves

$$\sum_\beta S_{\alpha\beta}X_\beta = g_\alpha = \frac{\partial\langle H\rangle}{\partial\overline{\theta_\alpha}}. \tag{15}$$

Here, $S_{\alpha\beta}$ is the quantum metric,[24] the unique metric on the variational manifold under which the geodesic distance between two points is proportional to the 2-norm distance between the corresponding quantum states in Hilbert space. It can be estimated via sampling

$$S_{\alpha\beta} = [\overline{O}_\alpha(\boldsymbol{s})O_\beta(\boldsymbol{s})] - [\overline{O}_\alpha(\boldsymbol{s})][O_\beta(\boldsymbol{s})]. \tag{16}$$

The quantum metric matrix $S$ is typically ill-conditioned. In practice, $\boldsymbol{X}$ is obtained by solving $(S+\varepsilon)\boldsymbol{X}=\boldsymbol{g}$, where $\varepsilon$ is a small regularization term.

## 4. Examples

### 4.1. Free fermion benchmark

We consider several paradigmatic free fermion examples to benchmark the VMC algorithm for fPEPS: the sublattice band insulator (Insulator), Dirac semimetal (Dirac), the $\phi = 2\pi/3$ Hofstadter model with Chern number 1 (Chern), and a system with a Fermi surface (Fermi)

$$H = -\sum_{\langle ij\rangle} t_{ij} c_i^\dagger c_j - \sum_i \mu_i c_i^\dagger c_i, \tag{17}$$

where $|t_{ij}| = 1$ in all systems. For the Chern model, the phases of $t_{ij}$ set the flux. For the Dirac model, vertical hoppings are 1 $(-1)$ along even (odd) columns, while horizontal hoppings are all 1. For the Insulator and Fermi models, all $t_{ij} = 1$. We set $\mu_i = \pm 1$ for the two sublattices in the Insulator; $\mu_i = 0$ for other models. For the Insulator, Dirac, and Fermi models, we fix the particle number at half-filling. For the Chern model, we fix the particle number at $2/3$ filling.

The hyperparameters of the VMC algorithm are listed in Table 1. Excessive fine-tuning is not required for these parameters.

**Table 1.** Hyperparameters used in the VMC.

| Parameter | Value |
|---|---|
| fPEPS bond dimension $D$ | 4 |
| bMPS bond dimension $D'$ | 12 (20 for Fermi) |
| SR regulator $\varepsilon$ | 0.001 |
| Step size $\delta$ | 0.1 |
| Number of samples | 4096 |
| Tensor initialization | random in [0,1] |

As shown in Fig. 2, the fPEPS VMC performs very well for the $10 \times 10$ insulator and Dirac models, as well as the $12 \times 12$ Chern model, achieving energy density errors on the order of $10^{-5}$. For the Fermi model, the calculation is more challenging, as expected, due to its large entanglement and high density of states near the ground state.

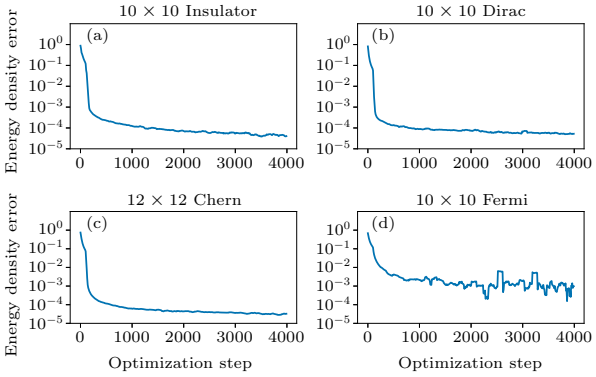



**Fig. 2.** Energy density error $\frac{E-E_{\text{exact}}}{L^2}$ as a function of VMC optimization steps. The data are presented as a moving average over every 100 steps. At each step, the energy is estimated by averaging over 4096 samples.

An interesting comparison is with boson PEPS representing the ground state of the fermion systems. Given a fixed computational basis, one may choose to represent the wavefunction amplitudes of the fermion system as a boson PEPS, without employing swap gates. To obtain the ground state, one needs to perform a JW transformation to construct a bosonic Hamiltonian and then run the bosonic algorithms. In the VMC algorithm, the long-rangeness of the JW string does not introduce any algorithmic difficulty in computing the energy gradient, since it is diagonal in the sampling basis. This contrasts with traditional PEPS methods, such as the simple or full update.[25–27] For the VMC algorithm, the difference between boson PEPS and fPEPS arises solely from the representational power of the ansatz. Because the fPEPS ansatz maintains locality under local gate actions, it is expected to provide a better approximation for the ground states of local fermion Hamiltonians, which is indeed observed in Fig. 3. In fact, the performance of boson PEPS is so poor that we could not even converge the calculation for a $10 \times 10$ system on the first attempts, so we illustrate results using $4 \times 4$ (and $6 \times 6$ for Chern) systems. We expect this difference to become even more pronounced for larger system sizes.

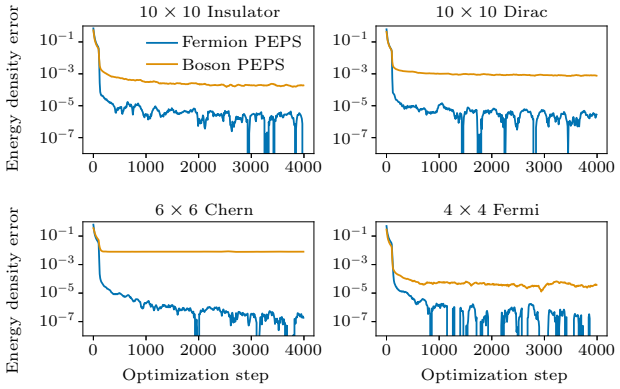



**Fig. 3.** Comparison between fermion PEPS and boson PEPS in terms of their performance in VMC for fermion systems. The energy density error $\frac{E-E_{\text{exact}}}{L^2}$ is shown as a function of VMC optimization steps. The data are presented as a moving average over every 100 steps. At each step, the energy is estimated by averaging over 4096 samples.

### 4.2. Hubbard model benchmark

We also include a benchmark on the $4 \times 4$ Hubbard model with $U = 8$ at half-filling. Its Hamiltonian is

$$H = -\sum_{\langle ij\rangle,\sigma} c_{i,\sigma}^\dagger c_{j,\sigma} + U \sum_i n_{i,\uparrow} n_{i,\downarrow}, \tag{18}$$

where $c_{i,\sigma}$ denotes the fermion annihilation operator on site $i$ with spin $\sigma = \uparrow$ or $\downarrow$. We work at half-filling, i.e., $\sum_i n_{i,\uparrow} = \sum_i n_{i,\downarrow} = 8$.

The VMC results are shown in Fig. 4. As seen, the energy error is significantly larger than in the free fermion models, indicating substantial entanglement. For comparison, a recent fPEPS study using exact gradient optimization and double-layer contraction reports an energy density error of $4 \times 10^{-3}$ with $SU(2)$ symmetry at $D = 6$, and $2 \times 10^{-2}$ with $U(1)$ symmetry at $D = 7$.[28]

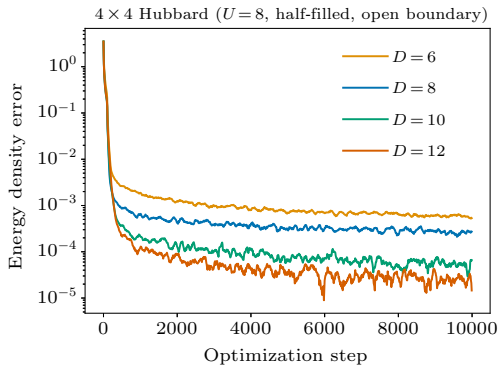



**Fig. 4.** Energy density error $\frac{E-E_{\text{exact}}}{L^2}$ as a function of VMC optimization steps for various bond dimensions $D$. Here, $D'$ is taken to be $4D$, and the other VMC hyperparameters are the same as in Table 1. The data are presented as a moving average over every 100 steps. At each step, the energy is estimated by averaging over 4096 samples. The exact energy $E_{\text{exact}} = -6.8084144664$ is obtained via exact diagonalization.

Another application of the current algorithm to the $8 \times 8$ Hubbard model with next-nearest-neighbor hopping at $1/8$ hole doping is reported in Ref. [29], with bond dimension $D = 10$, showing comparable accuracy to state-of-the-art neural quantum state ansatz.[29]

## 5. Conclusion

In this paper, we derived and explained the VMC algorithm for fermion PEPS in the swap gate formulation, highlighting its algorithmic simplicity and elegance. We also presented results demonstrating the effectiveness of the algorithm. In addition, we proved the detailed balance for sequential sampling, which has remained unclear in the field until now.

The main future direction of this work is the application of this algorithm to challenging interacting fermion systems, such as chiral spin liquids and superconductivity in the Hubbard model. Beyond applications, an important open question is to develop a framework where systems with a Fermi surface can be reliably simulated. This may require non-trivial modifications of the PEPS structure but should be possible within the flexible VMC framework.

## Acknowledgments

Part of the algorithm was tested using the TenPy code base.[30,31] Y.W. is supported by a startup grant from the IOP-CAS. Y.W. thanks Tao Xiang and Lei Wang for providing access to their computing resources. The data that support the findings of this article are openly available;[32] embargo periods may apply.

## References

[1] Loh E Y, Gubernatis J E, Scalettar R T, White S R, Scalapino D J and Sugar R L 1990 *Phys. Rev. B* **41** 9301
[2] Jordan P and Wigner E P 1928 *Z. Phys.* **47** 631
[3] White S R 1992 *Phys. Rev. Lett.* **69** 2863
[4] Kraus C V, Schuch N, Verstraete F and Cirac J I 2010 *Phys. Rev. A* **81** 052338
[5] Barthel T, Pineda C and Eisert J 2009 *Phys. Rev. A* **80** 042333
[6] Pizorn I and Verstraete F 2010 *Phys. Rev. B* **81** 245110
[7] Shi Q Q, Li S H, Zhao J H and Zhou H Q 2009 arXiv:0907.5520 [cond-mat.str-el]
[8] Corboz P, Orús R, Bauer B and Vidal G 2010 *Phys. Rev. B* **81** 165104
[9] Corboz P and Vidal G 2009 *Phys. Rev. B* **80** 165129
[10] Gu Z C, Verstraete F and Wen X G 2010 arXiv:1004.2563 [cond-mat.str-el]
[11] Liu W Y, Zhai H, Peng R, Gu Z C and Chan G K L 2025 *Phys. Rev. Lett.* **134** 256502
[12] Verstraete F and Cirac J I 2004 [arXiv:cond-mat/0407066]
[13] Lubasch M, Cirac J I and Bañuls M C 2014 *Phys. Rev. B* **90** 064425
[14] Liu W Y, Dong S, Wang C, Han Y, An H, Guo G C and He L 2018 *Phys. Rev. B* **98** 241109
[15] Liu W Y, Gong S S, Li Y B, Poilblanc D, Chen W Q and Gu Z C 2022 *Sci. Bull.* **67** 1034
[16] Liu W Y, Hasik J, Gong S S, Poilblanc D, Chen W Q and Gu Z C 2022 *Phys. Rev. X* **12** 031039
[17] Liu W Y, Gong S S, Chen W Q and Gu Z C 2024 *Sci. Bull.* **69** 190
[18] Liu W Y, Poilblanc D, Gong S S, Chen W Q and Gu Z C 2024 *Phys. Rev. B* **109** 235116
[19] Liu W Y, Zhang X T, Wang Z, Gong S S, Chen W Q and Gu Z C 2024 *Phys. Rev. Lett.* **133** 026502
[20] Liu W Y, Huang Y Z, Gong S S and Gu Z C 2021 *Phys. Rev. B* **103** 235155
[21] Dai Z, Wu Y, Wang T and Zaletel M P 2025 *Phys. Rev. Lett.* **134** 026502
[22] An fPEPS is a holomorphic ansatz
[23] Sorella S 1998 *Phys. Rev. Lett.* **80** 4558
[24] Provost J P and Vallee G 1980 *Commun. Math. Phys.* **76** 289
[25] Jiang H C, Weng Z Y and Xiang T 2008 *Phys. Rev. Lett.* **101** 090603
[26] Jordan J, Orús R, Vidal G, Verstraete F and Cirac J I 2008 *Phys. Rev. Lett.* **101** 250602
[27] Corboz P, Orús R, Bauer B and Vidal G 2010 *Phys. Rev. B* **81** 165104
[28] Scheb M and Noack R M 2023 *Phys. Rev. B* **107** 165112
[29] Gu Y, Li W, Lin H, Zhan B, Li R, Huang Y, He D, Wu Y, Xiang T, Qin M, Wang L and Lv D 2025 arXiv:2507.02644 [cond-mat.str-el]
[30] Hauschild J and Pollmann F 2018 *SciPost Phys. Lect. Notes* 5
[31] Hauschild J, Unfried J, Anand S, *et al.* 2024 *SciPost Phys. Codebases* 41
[32] Wu Y and Dai Z 2025 *GitHub Data Repository*